Taylor & Francis
Taylor & Francis Group

Ultrafast nuclear dynamics and non-uniform Coulomb explosion of heteroclusters*

J. JORTNER† and I. LAST

School of Chemistry, Tel Aviv University, Ramat Aviv, 69978 Tel-Aviv, Israel

This paper reports on some unique features of the ion spatial distribution, energetics and time-resolved dynamics in Coulomb explosion of multicharged light–heavy heteroclusters, consisting of light, low-charge and heavy, high-charge, ions, e.g. hydroiodic acid $(H^+I^{q_I+})_n$ and its isotopic substituents $(D^+I^{q_I+})_n$ and $(T^+I^{q_I+})_n$. In these clusters, extreme multielectron ionization in ultraintense laser fields (peak intensity $I = 10^{15} - 10^{20}\,W\,cm^{-2}$) results in highly charged heavy ions, e.g. $q_I \simeq 7$ at $I = 6 \times 10^{15}\,W\,cm^{-2}$ and $q_I = 25$ at $I = 10^{19}\,W\,cm^{-2}$. Molecular dynamics simulations based on the cluster vertical ionization (CVI) initial conditions, together with complete simulations involving both electron and nuclear dynamics of heteroclusters subjected to a Gaussian laser pulse, which were conducted for Coulomb explosion of $(D^+I^{q_I+})_{2171}$ and $(H^+I^{q_I+})_{2171}$ ionic clusters, reveal expanding, thin, two-dimensional spherical shells of the light D^+ or H^+ ions, with the monolayer expansion occurring on the femtosecond time scale. The expanding spherical nanoshells of light ions are analogous to a 'soap bubble', characterized by negative surface tension and driven by Coulomb pressure. The energetic data for the light ions reveal high energies with a narrow energy distribution, characterized by a lower energy cut-off, e.g. average energy $E_{av} = 23\,keV$ at width $\Delta E / E_{av} = 0.16$, and a cut-off energy of $E_{MIN} = 19.2\,keV$ for Coulomb explosion of $(D^+I^{q_I+})_{2171}$ clusters. These dynamic, structural and energetic data for exploding multicharged light–heavy heteroclusters arise from kinematic overrun effects of the light ions.

1. Prologue

Ultraintense table-top laser sources delivering $\sim 1\,J$ per pulse of ~ 10–$100\,fs$ are characterized by the power of ~ 10–$100\,TW$ $(10^{13}$–$10^{14}\,W)$ and by a maximal intensity of the focused beam of $\sim 10^{20}$–$10^{21}\,W\,cm^{-2}$, which constitutes the highest light intensity on earth [1]. Novel features of light–matter interactions emerge from the interaction of clusters with ultrashort (pulse temporal length $\tau = 10$–$100\,fs$) and ultraintense (peak intensity $I = 10^{15}$–$10^{20}\,W\,cm^{-2}$) laser fields [2–38]. The response of clusters to ultraintense laser fields is distinct from the electron–nuclear dynamic response of atoms, molecules, clusters and condensed matter in ordinary fields $(I \leqslant 10^{13}\,W\,cm^{-2})$, where perturbative quantum electrodynamics is applicable. It also differs from the response of 'small' atoms or molecules to ultraintense fields, which is triggered by a barrier suppression single-step mechanism [32–34]. When the cluster size exceeds the size of the laser field barrier distance of a single constituent, a new compound cluster ionization mechanism is manifested, which is driven by barrier suppression effects as well as by inner field ionic ignition and electron screening effects in the charged cluster [15, 16, 32, 34–37]. In the realm of matter–ultraintense laser interaction, the coupling of macroscopic dense matter, e.g. liquids and solids with ultraintense laser fields, is blurred by inhomogeneous dense plasma formation, isochoric heating, beam self-focusing and radiative continuum production effects [39–41]. However, the response of large finite systems, i.e. molecular systems, clusters or other nanostructures (whose size is considerably smaller than the laser wavelength) triggers well characterized ultrafast dynamics of electrons (on the time scale of ~ 1–$50\,fs$) and of nuclei of highly charged ions (on the time scale of 10–$100\,fs$) [2–38]. So, new avenues are opening up for the exploration of ultrafast (i.e. limited by the reciprocal laser frequency ν, i.e. $(2\pi\nu)^{-1} \sim 1$–$5\,fs$) electron and nuclear dynamics in ultraintense laser fields.

On the basis of our recent analyses and simulations [34–37], the electron dynamics of elemental and molecular clusters, such as $(Xe)_n$ [8, 11–22, 34, 35], $(D_2)_n$ and $(H_2)_n$ [24–28], $(D_2O)_n$ [25–27, 29] and $(CD_4)_n$ [30, 31, 37]

*This article is dedicated to Professor John Simons on the occasion of his 70th birthday.
†Corresponding author. Email: jortner@chemsg1.tau.ac.il

in ultraintense laser fields involves three sequential-parallel coupled processes of inner ionization, which results in the formation of a charged, energetic nanoplasma within the cluster (or its vicinity), and in (partial or complete) outer ionization of the nano-plasma. The yields and time-resolved dynamics of these three coupled electronic processes depend on the laser intensity, the pulse shape, the cluster size, and the electronic level structure of the cluster constituents [34–37]. The electron dynamics in ultraintense laser fields gives rise to novel, extreme multielectron cluster ionization [34, 35], involving the stripping of all electrons from light first-row atoms, and the formation of heavily charged ions, e.g. $(X^{q+})_n$ ($q = 8$–36), from heavy atoms. The electron dynamic processes trigger nuclear dynamics, with the outer ionization being accompanied by cluster Coulomb explosion [2–37], which results in the ultrafast (10–100 fs) formation of highly energetic (keV–MeV) multicharged ions. When the time scales for both inner ionization and outer ionization electronic processes are considerably faster than the nuclear dynamic process of Coulomb explosion, the cluster vertical ionization (CVI) approximation becomes valid [25, 34, 36, 37]. The CVI approximation, which implies that at the temporal onset of Coulomb explosion the inner and the outer ionization processes are already completed, decouples the dynamics of heavy particles (ions) from the dynamics of electrons. The spatially isotropic (or nearly so) cluster Coulomb explosion with the production of individual ions, which reflects on the Coulomb instability of multicharged systems, is realized for the Rayleigh fissibility parameter, $X = $ (Coulomb energy/2 surface energy) being $X > 1$, while for $X < 1$ cluster fission into large ionic fragments is manifested [42–45].

The traditional view of Coulomb explosion following cluster extreme multielectron ionization involves uni-form ion expansion [36], with the succession of the hierarchy of the ion distances from the cluster center being preserved during the explosion. Such uniform expansion prevails for Coulomb explosion of multi-charged homonuclear molecular or elemental clusters, e.g. $(D_2^{2+})_{n/2}$ ($\equiv (D^+)_n$), $(H_2^{2+})_{n/2}$ ($\equiv (H^+)_n$) or $(Xe^{q+})_n$, with the expansion of (e.g. D^+, H^+ or Xe^{q+}) ions retaining a uniform spatial distribution [36]. The situation is drastically different for Coulomb explosion of molecular heteroclusters, e.g. methane $(C^{q+}H_4^+)_n$ and $(C^{q+}D_4^+)_n$ ($q = 4$), where two subclusters are exhibited in Coulomb explosion [30, 37]. The spatial distribution manifests distinct radii for the expansion of the light (H^+ or D^+) subcluster ions, with (time-dependent) radii R_H or R_D, and for the expansion of the heavy C^{q+} ions, with $R_H(t)$ and $R_D(t) > R_C(t)$ at each t [37]. In this paper we explore the new and unique features of the spatial
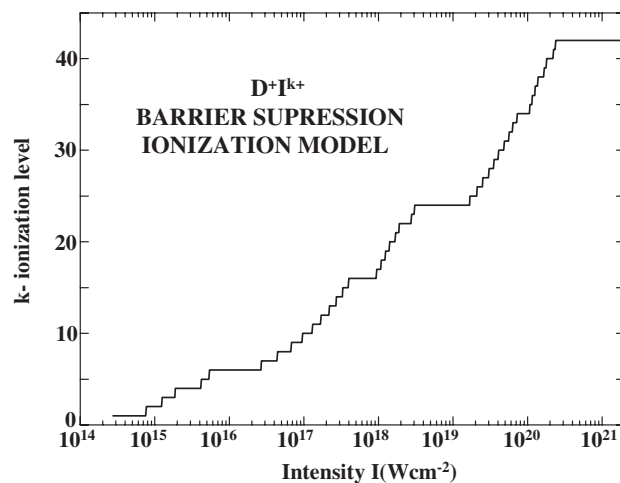

Figure 1. Laser intensity dependence of the ionization level of the DI molecule calculated by the barrier suppression ionization mechanism (BSI model [34]). Ionization potentials (IPs) of the ionic molecule were calculated with the IPs of the iodine atom taken from Carlson, Th. A., Nesta, C.W., Wasserman, N., and McDowel, J.D., *At. Data*, **2**, 63 (1970).

distribution, and the energetics and the time resolved dynamics of Coulomb explosion of highly ionized molecular heteroclusters $(A_k^{q_A+}B^{q_B+})_n$, which consist of light A^{q_A+} ions and heavy B^{q_B+} ions, e.g., hydroiodic acid clusters $(H^+I^{q_I+})_n$ or its isotopic substitutes $(D^+I^{q_I+})_n$ and $(T^+I^{q_I+})_n$. These will be referred to as light–heavy heteroclusters. Severe deviations from uni-form Coulomb explosion will be demonstrated in such heteroclusters. Extreme multielectron ionization levels, estimated from the barrier suppression ionization model [34] applied to DI and HI, exhibit high positive iodide ion charges, e.g. from $q_I = 7$ at $I = 6 \times 10^{15}$ W cm^{-2} to $q_I = 25$ at $I = 10^{19}$ W cm^{-2} and up to $q_I = 35$ at $I = 10^{20}$ W cm^{-2} (figure 1).

These single molecule extreme multielectron ioniza-tion data constitute a lower limit for the multielectron ionization level of the corresponding molecular cluster in the intensity range $I = 10^{17}$–10^{18} W cm^{-2}, where ignition effects [34, 35, 46, 47, 18] lead to the cluster size dependent enhancement of q_I in the cluster [34], while in the intensity range of 10^{19}–10^{20} W cm^{-2} the charges q_I on the individual cluster molecules are nearly identical to the single molecule q_I [48]. On the basis of molecular dynamics simulations in the CVI limit, and complete simulations involving both (highly energetic) electron and nuclear dynamics in an ultraintense laser field [34, 35] for multicharged light–heavy heteroclusters, we shall unveil new features of non-uniform Coulomb explosion, which give rise to ultrafast femtosecond dynamics of mobile, radial boundary, spherical monoionic shells of light ions.

2. Uniform Coulomb explosion of homonuclear clusters

Uniform Coulomb explosion prevails for multicharged homonuclear elemental and molecular clusters. When the initial CVI conditions are applicable, cluster Coulomb explosion of an $(A^{q_A+})_n$ cluster can be considered as a system consisting only of ions. This situation is physically realized at very high laser fields, i.e. $I \geqslant 10^{18}\,\mathrm{W\,cm^{-2}}$, which are initially located at the same geometry as the atoms in the neutral clusters [36, 41, 18]. The initial ion distribution is uniform and spherically symmetric [36, 41, 48]. This initial ion distribution is then approximated by a step function with a molecular (atomic) density $\rho(r_0) = \rho_0$ for $r_0 \leqslant R_0$ and $\rho(r_0) = 0$ for $r_0 > R_0$, where R_0 is the initial cluster radius, and by fixed and uniform ion charges ($q_i = q_A$, $i = 1, 2, \ldots, n$). The expansion of ions in these homonuclear clusters retains the uniform ion distribution, being described by the density $\rho(t)$ at $r \leqslant R(t)$, which is independent of r. $R(t)$ is the expanding cluster radius at time t. The uniform Coulomb explosion is, of course, characterized by a single radius of the expanding cluster. The distribution $P(E)$ of the kinetic energy E of the product ions is [26, 36]

$$
\begin{aligned}
P(E) &= (3/2E_M)(E/E_M)^{1/2}; & E \leq E_M, \\
P(E) &= 0; & E \geq E_M,
\end{aligned} \tag{1}
$$

with the maximal energy E_M provided by the periphery $r_0 = R_0$ ions being

$$
E_M = (4\pi/3)\bar{B}\rho_0 q_A^2 R_0^2. \tag{2}
$$

The average energy distribution obtained from the first moment of equation (1) is

$$
E_{av} = (3/5)E_M. \tag{3}
$$

In equation (2) and in what follows the lengths r_0, R_0 and $R(t)$ are expressed in Å, the density ρ_0 in Å^{-3}, the ionic charge q_A in e-units, the energies E, E_M and E_{av} in eV and $\bar{B} = 14.40\,\mathrm{eV\,Å}$. Equations (2) and (3) correspond to cluster size equations (CSE) [26, 30, 36]. Such scaling laws were advanced for a ubiquity of physical and chemical energetic, structural, dynamic and response observables to describe the convergence from finite systems to the infinite condensed phase [49–51]. The CSE for the energetics of Coulomb explosion is unique, as it diverges with R^2, being valid only for the finite cluster and not converging to the bulk value. To establish the validity of these analytical results we note that the energetic distribution in the Coulomb explosion of $(D)_n$ homonuclear clusters is well accounted for by equation (1) [36].

Uniform Coulomb explosion, which is characterized by the energy distribution $P(E) \propto E^{1/2}$ ($E < E_M$) and by $E_{av} \propto R_0^2$, according to equation (2), is well obeyed for homonuclear clusters [36]. For molecular heteroclusters deviations from uniform Coulomb explosion are ubiquitous, manifesting non-uniform spatial Coulomb explosion and a modification of the energy distribution, which were attributed to kinematic effects [25, 27, 30, 37]. The implications of kinematic effects on the Coulomb explosion of multicharged light–heavy heteroclusters will now be addressed.

3. Kinematic effects in the Coulomb explosion of heteroclusters

Invoking the CVI initial conditions we consider Coulomb explosion of light–heavy $(A_k^{q_A+}B^{q_B+})_n$ clusters, which consist of light A^{q_A+} ions with mass m_A and charge q_A, and heavy B^{q_B+} ions with mass m_B and charge q_B, where $m_A \ll m_B$ and $q_A \ll q_B$. The dynamics of the ion expansion is determined by the kinematic parameter [25, 27, 30, 37]

$$
\eta_{AB} = q_A m_B / q_B m_A. \tag{4}
$$

Typical values of η_{AB} for multicharged hydroiodic acid $(A^+I^{25+})_n$ clusters (A = H,D,T) are $\eta_{HI} = 5.1$ for H$^+$, $\eta_{DI} = 2.5$ for D$^+$ and $\eta_{TI} = 1.7$ for T$^+$. Such multicharged $(A^+I^{25+})_n$ clusters can be generated by extreme multielectron ionization at $I = 10^{18}\,\mathrm{W\,cm^{-2}}$ (figure 1). When $\eta_{AB} > 1$, the light A$^+$ ions overrun the heavy I^{25+} ions during the Coulomb expansion process. We shall now show that for $\eta_{AB} \gg 1$ the overrun process in Coulomb explosion of light–heavy heteroclusters results in the contraction of the spatial distribution of the expanding ions and in a narrow energy distribution of the light ions, which peak around the high value of their average kinetic energies.

Molecular dynamics (MD) simulations under CVI initial conditions were performed for Coulomb explosion of $(H^+I^{25+})_{2171}$ and $(D^+I^{25+})_{2171}$ light–heavy heteroclusters. These MD simulations encompass Coulomb interactions between all ions and the motion of both heavy and light ions. In figure 2 we pictorially present the time dependence of the spatial distribution of the light and heavy ions in Coulomb explosion of $(H^+I^{25+})_{2171}$. These results manifest:

(1) An overrun kinematic effect of the expanding light ions, which leaves the heavy ions behind.
(2) Two subclusters of light and heavy ions, respectively, are formed with a qualitatively different spatial structure.
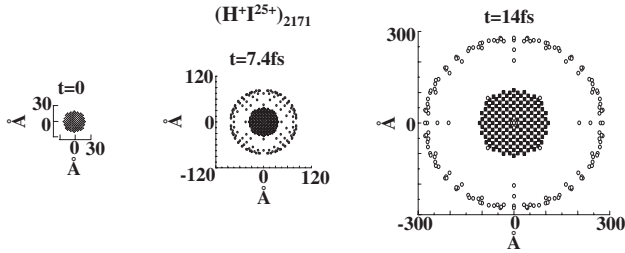
Figure 2. Two-dimensional pictures of the spatial configuration of Coulomb exploding $(H^+I^{25+})_{2171}$ light–heavy heteroclusters under CVI initial conditions at the times marked on the pictures. Black squares (■) represent I^{25+} ions, while circles (O) represent light H^+ or D^+ ions.

(3) The heavy ion subcluster retains nearly uniform small-scale spatial expansion.

(4) The ionic subcluster of the heavy atoms drives away the light ions.

(5) A narrow shell of expanding light ions is formed. The unique features of the spatial structure of this light ions subcluster bear analogy to expanding "soft matter" [44].

MD simulations under initial CVI conditions unveil some quantitative novel features of the expanding narrow shells of the light ions. Figures 3 and 4 portray the radial distribution $P(r)$ for the light H^+ and D^+ ions in Coulomb explosion of $(H^+I^{25+})_{2171}$ and $(D^+I^{25+})_{2171}$ clusters, respectively. These $P(r)$ data manifest the femtosecond dynamics of the spherically expanding narrow shells of H^+ and of D^+, which provide an extreme case of non-uniform Coulomb explosion of light–heavy heteroclusters. In the insets to figures 3 and 4 we present the time dependence of the mean radii R_H and R_D of the expanding shell of the light H^+ and D^+ ions, respectively, the radius R_I of the expanding heavy I^{25+} ion subclusters, the widths ΔR of the H^+ and D^+ ion expanding shells (defined as the $P(r)$ domain around the distribution maximum containing 50% of the light ions) and the mean distances d between the light ions. From these results we infer that:

(1) The characteristic times, t_v, for the attainment of very narrow shells after the onset of Coulomb explosion, are $t_v = 4.1\,\mathrm{fs}$ for H^+ and $t_v = 7.4\,\mathrm{fs}$ for D^+. These values of t_v manifest a normal isotope effect of the form $\sim m_A^{1/2}$ (figures 3 and 4).

(2) The mean radii R_H ($\sim 700\,\mathrm{\AA}$ at $t = 30\,\mathrm{fs}$) and R_D ($\sim 600\,\mathrm{\AA}$ at $t = 40\,\mathrm{fs}$) for the expansion of the light H^+ and D^+ shells, respectively, exhibit a linear time dependence for $t > t_v$ (insets to figures 3 and 4).

(3) The time dependence of the mean radii of the light ion shells and of the heavy ion subclusters in the non-uniform Coulomb explosion of $(H^+I^{25+})_{2171}$ at $t > t_v$ (inset to figure 3) are: $dR_H/dt = 21.7\,\mathrm{\AA\,fs^{-1}}$
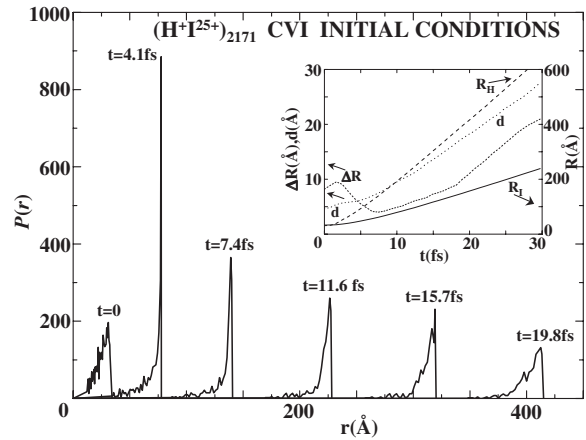

Figure 3. Molecular dynamics simulations under CVI initial conditions of Coulomb explosion of $(H^+I^{25+})_{2171}$ heteroclusters, representing the ultrafast (fs) time dependence of the spatial distribution $P(r)$ of the H^+ ions at the times marked on the curves. The insert shows the time dependence of the mean radius (the first moment of $P(r)$) of the H^+ ions (R_H) and of the I^{25+} ions (R_I), the distribution width ΔR and the average interionic distance d between the H^+ ions.
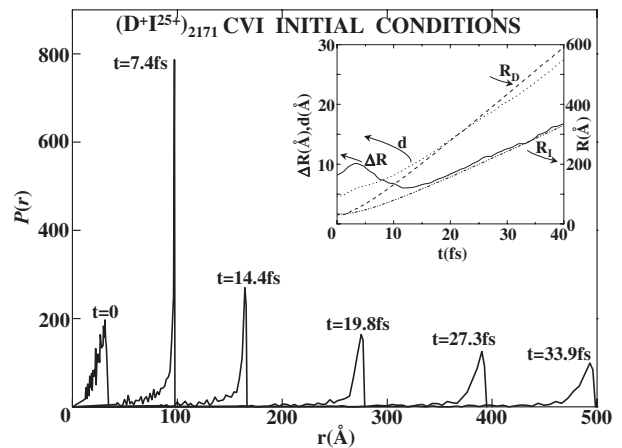

Figure 4. Molecular dynamics simulations under CVI initial conditions of Coulomb explosion of $(D^+I^{25+})_{2171}$ heteroclusters, representing the ultrafast (fs) time dependence of the spatial distribution $P(r)$ of the D^+ ions at the times marked on the curves. The insert shows the time dependence of the mean radius (first moment of $P(r)$) of the distribution of the D^+ ions (R_D) and of the I^{25+} ions (R_I), the distribution width ΔR and the average interionic distance d between the D^+ ions.

and $dR_I/dt = 8.0\,\mathrm{\AA\,fs^{-1}}$, while for $(D^+I^{25+})_{2171}$ the corresponding values (inset to figure 4) are: $dR_D/dt = 15.0\,\mathrm{\AA\,fs^{-1}}$ and $dR_I/dt = 8.0\,\mathrm{\AA\,fs^{-1}}$. The expansion rates of the light ion shells exhibit an isotope effect ($\sim m_A^{1/2}$), in accord with the pictorial data of figure 2, while the expansion rates of the heavy ion subclusters are independent of the isotopic species of the light ions.

(4) The shell widths ΔR of the H^+ and D^+ ions (insets to figures 3 and 4) first slightly increase and soon start to decrease, attaining a maximum at $t \sim 3$ fs for H^+ shells and at $t = 4$ fs for D^+ shells. A shallow minimum in ΔR is exhibited at 3 Å at $t_{MIN} = 7$ fs for H^+ shells and at 4 Å at $t_{MIN} = 12$ fs for D^+ shells. Subsequently, the ΔR values start to increase with time, with $(d\Delta R/dt)_D = 0.40$ Å fs^{-1} for the expansion of D^+ ion shells (inset to figure 4), while the expansion of H^+ ion shells (inset to figure 3) exhibits a linear time dependence in the range $t = 10$–20 fs with $(d\Delta R/dt)_H = 0.47$ Å fs^{-1}.

(5) From the foregoing analysis of the time dependence of ΔR (point (4) above) we conclude that at $t > t_{MIN}$ the narrow shells of H^+ and D^+ ions slowly begin to broaden, with the shell structure of the light ion subclusters being preserved.

(6) The expansion rates of the widths of the narrow shells exhibit an isotope effect, decreasing with increasing the mass of the light ion.

(7) A narrow shell structure is preserved, i.e., $(\Delta R/R)_H = 0.022$ and $(\Delta R/R)_D = 0.027$, over the longer time domain where the time dependence of both R and ΔR is linear. These estimates quantify the narrow shell expanding structure.

(8) The average interatomic distance d at short times $t < t_{MIN}$ is lower than ΔR, while at longer times when $t \gtrsim t_{MIN}$, d exceeds ΔR. When $d > \Delta R$ over a broad time domain of $t > t_{MIN}$ (insets to figures 3 and 4), the expanding light ion shells correspond to a two-dimensional monolayer expansion.

The MD simulations under CVI initial conditions reveal expanding, thin, two-dimensional shells of light H^+ and D^+ ions, with the monolayer expansion occurring on the femtosecond time scale. Under CVI conditions the role of electron dynamics on the nuclear dynamics is disregarded. In order to explore the effects of electron dynamics on Coulomb explosion of light–heavy heteroclusters, we performed simulations of Coulomb explosion time-dependent spatial distribution of the light ions by complete simulations including both (high energy) electron and nuclear dynamics in clusters coupled to ultraintense laser fields [15, 26, 34–37]. This simulation scheme (referred to as E+N simulations) was recently developed [34]. These high energy ($\sim$1–50 keV) electron dynamics in the highest intensity range of $I = 10^{19}$–10^{20} W cm^{-2} also incorporate relativistic effects and include laser magnetic field effects [34]. The E+N simulation scheme was applied to an $(HI)_{2171}$ cluster subjected to a Gaussian laser pulse with the laser electric field

$$F_l(t) = F_{l0}(t) \cos(2\pi \nu t + \phi_0) \qquad (5)$$
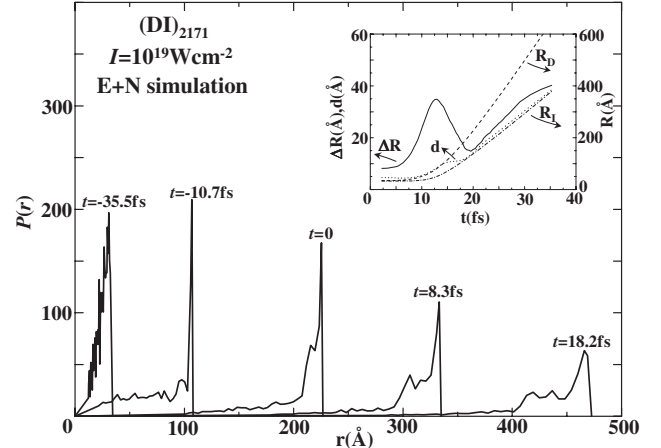

Figure 5. E+N simulations of Coulomb explosion in $(DI)_{2171}$ heteroclusters subjected to a Gaussian laser field with peak intensity $I = 10^{25}$ W cm^{-2}, pulse width $\tau = 25$ fs and temporal pulse onset at $t_s = -35.5$ fs. The curves present the spatial distributions $P(r)$ of the light ions at times t, marked on the curves, with the first curve obtained at $t = t_s$. The insert shows the time dependences of R_D, R_I, ΔR and d defined in figures 3 and 4.

(for $-\infty \leqslant t \leqslant \infty$), with frequency $\nu = 0.35$ fs^{-1} (photon energy 1.44 eV) and phase $\phi_0 = 0$, where $F_{l0}(t)$ is the laser field envelope

$$F_{l0}(t) = F_M \exp\left[-2.773(t/\tau)^2\right] \qquad (6)$$

with F_M being the maximal electric field (which is related to the laser peak intensity by $eF_M = 2.75 \times 10^{-7} I^{1/2}$ eV Å^{-1}), and $\tau (=25$ fs) being the pulse temporal width. The laser peak intensity was taken as $I = 10^{19}$ W cm^{-2}. At this intensity the ionization level of the iodine atoms is $q_I = 25$ (figure 1), being the same as in our CVI molecular dynamics simulations. The light ion shell structure for the complete simulations (figure 5) is somewhat broader (by a numerical factor of $\sim$2) than the CVI simulation results, i.e. $(\Delta R/R)_D = 0.06$ in the linear range (insert to figure 5), as compared to $(\Delta R/R)_D = 0.027$ for the CVI simulations (figures 3 and 5). This difference manifests the role of outer ionization electron dynamics. At an advanced expansion stage, the shell of the light ions manifests a bimodal distribution (figure 5) reflecting the presence of faster ions (higher maximum) and slower ions (lower maximum), which is also exhibited in the energy distribution $P(E)$, and which will be considered subsequently in section 4. The general character of the time dependence of ΔR and d is similar to that of the CVI simulations portrayed in the inserts to figures 3 and 4. In particular, for longer times in the linear increasing range of ΔR and of d, we note that $d > \Delta R$ (insert to figure 5), so that the two-dimensional shell structure is preserved.

4. Energetics of non-uniform Coulomb explosion of light–heavy heteroclusters

Within the framework of the CVI, we advance a simple electrostatic model for Coulomb explosions of light–heavy $A_k^{q_A+}B^{q_B+}$ heteroclusters. For these heteroclusters we impose two approximations. First, as $kq_A \ll q_B$, we shall ignore the light ion charge. Second, as $\eta_{AB} \gg 1$, we shall ignore the heavy ion motion on the time scale of the light ion motion through the B^{q_B+} ion motion. A simple electrostatic consideration provides the potential for an A^{q_A+} ion

$$U(r) = (2\pi/3)\bar{B}\rho_0 q_B q_A (3R_0^2 - r^2); \quad r \le R_0, \quad (7)$$

$$U(r) = (4\pi/3)\bar{B}\rho_0 q_B q_A R_0^3/r; \quad r > R_0 \quad (8)$$

where R_0 is the initial heterocluster radius and ρ_0 is the initial molecular density of A_kB within the cluster. The final kinetic energy $E(r_0)$ of an A^{q_A+} ion initially located at $r_0 \le R_0$, is $E(r_0) = U(r_0)$, whereupon

$$E(r_0) = [3 - (r_0/R_0)^2]E_{MIN}/2 \quad (9)$$

with the minimal energy being

$$E_{\mathrm{MIN}} = (4\pi/3)\bar{B}\rho_0 q_B q_A R_0^2. \quad (10)$$

The energy distribution of the final energies of the light ions is derived from equation (8) in the form

$$P(E) = (3/E_{\mathrm{MIN}})[3 - 2(E/E_{\mathrm{MIN}})]^{1/2};$$
$$E_{\mathrm{MIN}} \le E \le \frac{3}{2}E_{\mathrm{MIN}} \quad (11)$$

and the average energy is

$$E_{\mathrm{av}} = (6/5)E_{\mathrm{MIN}}. \quad (12)$$

The average energy, equation (12), and the energy distribution, equation (11), for non-uniform Coulomb explosion of the light-heavy heterocluster quantitatively differ from the energetics of non-uniform Coulomb explosion of homonuclear clusters, equations (1) and (3). The major differences between these two distinct physical situations pertain to the existence of a lower, finite minimal energy E_{MIN} in $P(E)$ and a narrow energy distribution of $\sim E_{\mathrm{MIN}} = (5/12)E_{\mathrm{av}}$ in the non-uniform Coulomb explosion of light–heavy heteroclusters, while for homonuclear clusters the energy distribution spans the entire range $0 < E \le E_{\mathrm{M}}$. These unique features of the energy distribution from light–heavy heteroclusters are due to kinematic effects, with the light A^{q_A+} ions from the inner region of the cluster ($r_0 < R_0$) over-running the heavy ion core, and gaining a higher energy
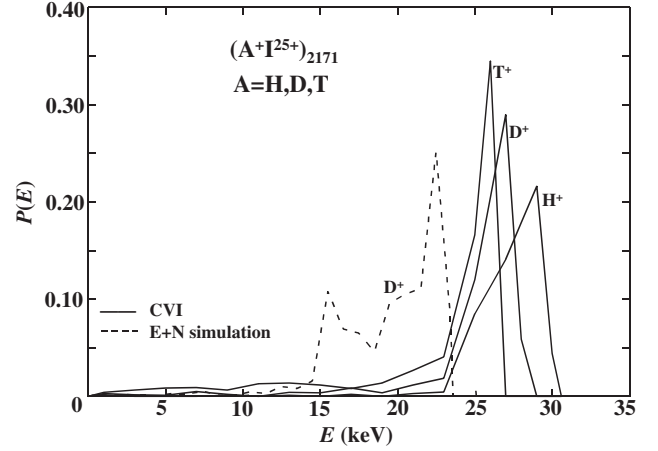

Figure 6. Kinetic energy distributions $P(E)$ of light ions in Coulomb explosion of extremely multicharged hydroiodic acid and its isotopic species. The solid curves represent molecular dynamics simulations $P(E)$ of A^+ ions from Coulomb explosion of $(A^+I^{25+})_{2171}$ heteroclusters (A = H,D or T) under CVI initial conditions. The dashed curves represent kinetic energy distributions obtained from E + N simulations in $(DI)_{2171}$ heteroclusters subjected to a Gaussian laser field with $I = 10^{19}\,\mathrm{W\,cm^{-2}}$, $\tau = 25\,\mathrm{fs}$, and a temporal onset of the laser at $t_s = -35.5\,\mathrm{fs}$, using the procedure of references [34] and [35].

than the periphery A^{q_A+} ions ($r_0 = R_0$). Consequently, the periphery light ions provide a minimum energy, equation (10), in contrast to the case of uniformly expanding homonuclear clusters, equations (1) and (3).

MD simulations of the energetics of Coulomb explosion with CVI initial conditions were performed for the heteronuclear $(A^+I^{25+})_{2171}$ clusters (A = H, D and T). The simulation results confirm the narrow energy distribution (figure 6) predicted by equation (11). In contrast to the theoretical model, equations (7) and (8), the CVI simulations reveal an isotope effect (figure 6), which originates from the (slow) motion of the heavy ions. The energy distribution width, ΔE, which includes 75% of the ions, is rather narrow, corresponding to $\Delta E = 0.14E_{\mathrm{av}}$, $0.13E_{\mathrm{av}}$, and $0.16E_{\mathrm{av}}$ for H^+, D^+ and T^+ ions, respectively. These simulated values of ΔE are lower than the value of $\Delta E = 0.25E_{\mathrm{av}}$ obtained from the theoretical distribution, equation (11). Together with the CVI energy distributions, we also display in figure 6 the energy distribution obtained by a complete E + N simulation for a $(DI)_{2171}$ cluster interacting with a Gaussian laser pulse of $I = 10^{19}\,\mathrm{W\,cm^{-2}}$, width $\tau = 25\,\mathrm{fs}$ and temporal of onset $t_s = -35.3\,\mathrm{fs}$. The D^+ ion energy obtained by E + N simulations, $E_{\mathrm{av}} = 19.5\,\mathrm{keV}$, is smaller than the CVI energy of $E_{\mathrm{av}} = 25.5\,\mathrm{keV}$, the decrease being due to the coupling between outer ionization electron dynamics and Coulomb explosion nuclear dynamics induced by

the Gaussian pulse [36]. The energy distribution provided by the E + N simulations shows that $P(E)$ is wider than in the case of CVI simulations and exhibits two peaks. These features are due to finite-time outer ionization effects [35, 36]. The width of this energy distribution is, however, still relatively narrow, being $\Delta E = 0.33 E_{\text{av}}$.

5. Epilogue

Molecular dynamics simulations based on CVI initial conditions and on E+N simulations of electron and nuclear dynamics for Coulomb explosion of extremely charged light–heavy heteroclusters reveal mobile, 2–dimensional, thin spherical shells of the light ions, which expand on the femtosecond time scale, and which originate from kinematic overrun effects. Direct information on transient structures, i.e. the mapping of all nuclear coordinates involved in a dynamic process, unveils new facets of ultrafast (timescales of ns to fs) dynamics in chemistry, physics and biology [52–55]. Our predictions of unique transient structures for multi-charged, thin, unimolecular spherical shells expanding on the fs time scale, introduce a family of new transient ultrafast dynamics of clusters, which should be subjected to experimental scrutiny. Two general experimental approaches were advanced involving X-ray absorption and diffraction (on the ns time scale) [53, 55] and ultrafast electron diffraction (on the fs–ps time scale) [54]. Our results provide the conceptual basis for future experimental studies of these unique femtosecond transient structures of exploding homonuclear clusters, using the experimental ultrafast electron diffraction methods pioneered by Zewail *et al.* for transient, molecular structures [54] in photochemical reactions in complex molecules. As the radial distribution function for this transient structure involves two sharp, spatial distributions separated by $R \approx 100\,\text{Å}$ (figures 2–4), low energy electrons ($\sim$100–300 eV) have to be utilized.

Another experimental prediction emerging from the present model and from simulations for Coulomb explosion of multicharged light-heavy heteroclusters pertains to the energy distribution of the light ions, i.e. protons or deuterons (figure 6). According to equations (10)–(12), the sharp energy distribution spans a narrow energy range $E_{\text{MIN}} \leqslant E \leqslant 3E_{\text{MIN}}/2$, with a low energy cut-off at $E_{\text{MIN}} = 5E_{\text{av}}/6$. This unique energy distribution is predicted to prevail under CVI conditions, with the temporal onset of Coulomb explosion, which is obtained after the completion of the inner and the outer ionization processes. A criterion for the validity of the CVI conditions was advanced [36, 37] in terms of an intensity-dependent 'critical' radius $(R_0)_I$, i.e. $R_0 < (R_0)_I$,

which ensures the completion of inner ionization and the realization of the cluster size equation $E_{\text{MIN}} \propto R_0^2$ scaling law [36, 37]. For $R_0 > (R_0)_I$ outer ionization and Coulomb explosion temporarily overlap, with the lower limit E_{MIN} for the energy distribution of the light ions being smeared out towards lower energies and the low energy threshold being eroded. Experimental results for the ion energies in Coulomb explosion of $(HI)_n$ ($n = 6 \times 10^4$ and $R_0 = 102\,\text{Å}$) at the laser intensity of $I = 2 \times 10^{16}\,\text{W cm}^{-2}$ [38] revealed a continuous distribution of the proton energy in the range 0.1–3.0 keV, without any indication of a low energy threshold. For the intensities employed by Tisch and his colleagues [38], the 'critical' $(HI)_n$ cluster radius for the realization of CVI conditions is $(R_0)_I = 11\,\text{Å}$ at $I = 2 \times 10^{16}\,\text{W cm}^{-2}$, as inferred from an analysis of Xe_n clusters [48], which are isoelectronic with $(HI)_n$. Accordingly, the cluster radius $R_0 = 102\,\text{Å}$ of the $(HI)_n$ cluster studied by Tisch *et al.* [38] is overwhelmingly larger than $(R_0)_I = 11\,\text{Å}$ and the CVI condition, which serves as a cornerstone for the present analysis, breaks down. The disagreement between the present theory and the available experimental data [38] reflects on a distinct physical situation for electron and nuclear dynamics. While the theory addressed complete outer ionization, i.e. $R_0 < (R_0)_I$, the experimental data correspond to parallel outer ionization and Coulomb explosion, i.e. $R_0 \gg (R_0)_I$. It will be interesting to provide an experimental test of our theory by the investigation of the energy distribution of the light ions in Coulomb explosion of multicharged light-heavy heteroclusters under the conditions $R_0 < (R_0)_I$, i.e. for ultrahigh laser intensities of $I = 10^{18}–10^{19}\,\text{W cm}^{-2}$. For $(HI)_n$ clusters, we estimate [48] that $(R_0)_I = 30\,\text{Å}$ at $I = 10^{18}\,\text{W cm}^{-2}$ and that $(R_0)_I = 85\,\text{Å}$ at $I = 10^{19}\,\text{W cm}^{-2}$, setting the upper bounds on the cluster radii for the applicability of the CVI conditions.

Further insight into the nature of the expansion of such thin two-dimensional light ion spheres (figures 2–5) can be obtained from a slight extension of the electrostatic model of section 4. The potential energy, U, of the thin sphere of radius $R \gg R_0$, with $\Delta R \ll R$, is taken as the sum of light ion–heavy ion potential energy U_{LH} and light ion–light ion potential energy U_{LL}. From equation (8) we obtain $U_{\text{LH}} = nkE_{\text{MIN}}R_0/R$, while a straightforward estimate gives $U_{LL} = \bar{B}(nkq_A)^2$. The condition $U_{\text{LH}} \gg U_{\text{LL}}$ implies that $kq_A \ll q_B$, in accord with the approximate electrostatic model of section 4. The potential energy is now

$$U = \bar{B}n^2 kq_A q_B/R + \bar{B}(nk)^2 q_A^2/R. \qquad (13)$$

The first term in equation (13) corresponds to the pressure (p)–volume (V) energy term, while the second

term corresponds to the surface tension (γ)–surface energy (s) term. The energy change is

$$dU = -pdV + \gamma ds \qquad (14)$$

where the negative sign for the pdV term represents internal pressure from inside the sphere. The pressure $p = -(\partial U/\partial V)_s$ is given by

$$p = \bar{\mathbf{B}}(n^2 k/4\pi)q_A q_B/R^4. \qquad (15)$$

The pressure originates from light ion–heavy ion repulsions. The surface tension $\gamma = (\partial U/\partial s)_v$ is given by

$$\gamma = -\bar{\mathbf{B}}(n^2 k^2/8\pi)q_A^2/R^3. \qquad (16)$$

The surface tension, due to light ion–light ion repulsion, is negative. The expanding, two-dimensional, thin spherical shell of light ions is analogous to a 'soap bubble' with a negative surface tension, which is driven by Coulomb pressure. The unique features of Coulomb instability of highly charged light–heavy heteroclusters opens up new avenues for the exploration of transient, soft, regular 'nanointerfaces'.

Acknowledgements

References

[1] G.A. Mourou, C.P.J. Barty, M.D. Perry. *Phys. Today*, **51**, 22 (1998).

[2] K. Boyer, T.S. Luk, J.C. Solem, C.K. Rhodes. *Phys. Rev. A*, **39**, 1186 (1989).

[3] J. Purnell, E.M. Sayder, S. Wei, A.W. Castleman Jr. *Chem. Phys. Lett.*, **229**, 333 (1994).

[4] T. Ditmire, J.W.G. Tisch, E. Springate, M.B. Mason, N. Hay, R.A. Smith, J. Marangos, M.H.R. Hutchinson. *Nature*, **386**, 54 (1997).

[5] T. Ditmire, E. Springate, J.W.G. Tisch, Y.L. Shao, M.B. Mason, N. Hay, J.P. Marangos, M.H.R. Hutchinson. *Phys. Rev. A*, **57**, 369 (1998).

[6] J.V. Ford, O. Zhong, L. Poth, A.W. Castleman Jr. *J. chem. Phys.*, **110**, 6257 (1999).

[7] M. Lezius, V. Blanchet, D.M. Rayner, D.M. Villeneuve, A. Stolov, M. Yu. Ivanov. *Phys. Rev. Lett.*, **86**, 51 (2001).

[8] E. Springate, N. Hay, J.W.G. Tisch, M.B. Mason, T. Ditmire, M.H.R. Hutchinson, J.P. Marangos. *Phys. Rev. A*, **57**, 063201 (2000).

[9] D.A. Card, E.S. Wisniewski, D.E. Folmer, A.W. Castleman Jr. *J. chem. Phys.*, **116**, 3554 (2002).

[10] T. Ditmire, J.W.G. Tisch, E. Springate, M.B. Mason, N. Hay, J.P. Marangos, M.H.R. Hutchinson. *Phys. Rev. Lett.*, **78**, 2832 (1997).

[11] T. Ditmire, R.A. Smith, J.W.G. Tisch, M.H.R. Hutchinson. *Phys. Rev. Lett.*, **78**, 3121 (1997).

[12] K. Kondo, A.B. Borisov, C. Jordan, A. McPherson, W.A. Schroeder, K. Boyer C.K. Rhodes. *J. phys.* B, **30**, 2707 (1997).

[13] M. Lezius, S. Dobosz, D. Normand, M. Schmidt. *Phys. Rev. Lett.*, **80**, 261 (1998).

[14] I. Last, J. Jortner. *Phys. Rev. A*, **60**, 2215 (1999).

[15] I. Last, J. Jortner. *Phys. Rev. A*, **62**, 013201 (2000).

[16] K. Ishikava, T. Blenski. *Phys. Rev. A*, **62**, 063204 (2000).

[17] K.J. Mendham, N. Hay, M.B. Mason, J.W.G. Tisch, J.P. Marangos. *Phys. Rev. A*, **64**, 055201 (2001).

[18] C. Siedschlag, J.M. Rost. *Phys. Rev. A*, **67**, 013404 (2003).

[19] V. Kamarappan, M. Krishnamurthy, D. Mathur. *Phys. Rev. A*, **67**, 043204 (2003).

[20] Y. Fukuda, K. Yamakawa, Y. Akahane, M. Aoyama, N. Inoue, H. Ueda, Y. Kishimoto. *Phys. Rev. A*, **67**, 061201 (2003).

[21] I. Last, J. Jortner. *Z. Phys. Chem.*, **217**, 975 (2003).

[22] M. Schnürer, S. Ter-Avetisyan, H. Stiel, U. Vogt, W. Radloff, M. Kalashnikov, W. Sandner, P.V. Nickles. *Eur. Phys. J. D*, **14**, 331 (2001); S. Ter-Avetisyan, U. Vogt, H. Stiel, M. Schnürer, I. Will, P.V. Nickles. *J. appl. Phys.*, **94**, 1 (2003).

[23] J. Zweiback, R.A. Smith, T.W. Cowan, G. Hays, K.B. Wharton, V.P. Yanovsky, T. Ditmire. *Phys. Rev. Lett.*, **84**, 2634 (2000).

[24] J. Zweiback, T.E. Cowan, R.A. Smith, J.H. Hurtlay, R. Howell, C.A. Steinke, G. Hays, K.B. Wharton, J.K. Krane, T. Ditmire. *Phys. Rev. Lett.*, **85**, 3640 (2000).

[25] I. Last, J. Jortner. *Phys. Rev. Lett.*, **87,** 033401 (2001).

[26] I. Last, J. Jortner. *Phys. Rev.*, **64**, 063201 (2001).

[27] J. Jortner, I. Last. *Chem. Phys. Chem.*, **3**, 845 (2002).

[28] R.W. Madison, P.K. Patel, M. Allen, D. Price, R. Fitzpatrick, T. Ditmire. *Phys. Plasmas*, **11**, 1 (2004).

[29] V. Kumarappan, M. Krishnamurthy, D. Mathur. *Phys. Rev. A*, **67**, 063207 (2003).

[30] I. Last, J. Jortner. *J. Phys. Chem. A*, **106**, 10877 (2002).

[31] G. Grillon, Ph. Balcou, J.-P. Chambaret, D. Hulin, J. Martino, S. Moustaizis, L. Notebaert, M. Pittman, Th. Pussieux, A. Rousse, J-Ph. Rousseau, S. Sebban, O. Sublemontier, M. Schmidt. *Phys. Rev. Lett.*, **89**, 065005 (2002).

[32] T. Ditmire. *Phys. Rev. A*, **57**, R4094 (1998).

[33] V.P. Krainov, M.B. Smirnov. *Phys. Rep.*, **370**, 237 (2002).

[34] I. Last, J. Jortner. *J. chem. Phys.*, **120**, 1336 (2004).

[35] I. Last, J. Jortner. *J. chem. Phys.*, **120**, 1348 (2004).

[36] I. Last, J. Jortner. *J. chem. Phys.*, **121**, 3030 (2004).

[37] I. Last, J. Jortner. *J. chem. Phys.*, **121**, 8329 (2004).

[38] J.W.G. Tisch, N. Hay, V. Springate, E.T. Gumprell, M.H.R. Hutchinson, J.P. Marangos. *Phys. Rev. A*, **60**, 3076 (1999).

[39] R.A. Snavely, et al. *Phys. Rev. Lett.*, **85**, 2945 (2000).

[40] C. Gaha, G.D. Tsakiris, G. Pretzler, K.J. Witte, C. Delfin, C.-G. Wahlström, D. Habs. *Appl. Phys. Lett.*, **80**, 198 (2002).

[41] R. Storian, A. Rosenfeld, D. Ashkenasi, I.V. Hertel, N.M. Bulgakova, E.B. Campbell. *Phys. Rev. Lett.*, **88**, 097603 (2002).

[42] I. Last, I. Schek, J. Jortner. *J. chem. Phys.*, **107**, 6685 (1997).

[43] I. Last, Y. Levy, J. Jortner. *Proc. Natl. Acad. Sci.* USA, **99**, 9107 (2002).

[44] U. Näher, S. Bjornholm, S. Fraundorf, F. Gracias, C. Guet. *Phys. Rep.*, **285**, 245 (1997).

[45] Y. Levy, I. Last, Jortner, J. (in preparation).

[46] C. Rose-Petruck, K.J. Schafer, K.R. Wilson, C.P.J. Barty. *Phys. Rev.* A, **55**, 1182 (1997).

[47] D. Bauer, A. Macchi. *Phys. Rev.* A, **68**, 033201 (2003).

[48] A. Heidenreich, I. Last, Jortner, J. (in preparation).

[49] J. Jortner. *Z. Phys.* D., **24**, 247 (1992).

[50] N. Ben-Horin, J. Jortner. *J. chem. Phys.*, **98**, 9346 (1993).

[51] J. Jortner. *J. chem. Phys.*, **92**, 205 (1995).

[52] Y. Tanimura, K. Yamashita, P.A. Anfunrud. *Proc. Natl. Acad. Sci.* USA, **96**, 8823 (1999).

[53] J.R. Helliwell, P.M. Rentzepis, (Eds.), *Time-resolved Diffraction*, Oxford University Press, New York (1997).

[54] H. Ihee, V. Lostov, U.M. Gomez, B.M. Goodson, R. Srinivasan, C.Y. Ruan, A.H. Zewail. *Science*, **291**, 458 (2001).

[55] L.X. Chen, W.J.H. Jäger, G. Jennings, D.J. Gosztola, A. Munkholm, J.P. Hessler. *Science*, **292**, 262 (2001).